Capacitance and Conductance for an MOS System in Inversion, with Oxide Capacitance and Minority Carrier Lifetime Extractions

Scott Monaghan, *Senior Member, IEEE*, Éamon O'Connor, Rafael Rios, *Senior Member, IEEE*, Fahmida Ferdousi, Liam Floyd, Eimear Ryan, Karim Cherkaoui, Ian M. Povey, Kelin J. Kuhn, *Fellow, IEEE*, and Paul K. Hurley, *Member, IEEE*

***Abstract*— Experimental observations for the $In_{0.53}Ga_{0.47}As$ metal–oxide–semiconductor (MOS) system in inversion indicate that the measured capacitance (C) and conductance (G or G_m), are uniquely related through two functions of the alternating current angular frequency (ω). The peak value of the second function ($-dC/d\log_e(\omega) \equiv -\omega dC/d\omega$) is equal to the peak value of the first function (G/ω). Moreover, these peak values occur at the same angular frequency (ω_m), that is, the transition frequency. The experimental observations are confirmed by physics-based simulations, and applying the equivalent circuit model for the MOS system in inversion, the functional relationship is also demonstrated mathematically and shown to be generally true for any MOS system in inversion. The functional relationship permits the discrimination between high interface state densities and genuine surface inversion. The two function peak values are found to be equal to $C_{ox}^2/(2(C_{ox}+C_D))$ where C_{ox} is the oxide capacitance per unit area and C_D is the semiconductor depletion capacitance in inversion. The equal peak values of the functions, and their observed symmetry relation about ω_m on a logarithmic ω plot, opens a new route to experimentally determining C_{ox}. Finally, knowing ω_m permits the extraction of the minority carrier generation lifetime in the bulk of the $In_{0.53}Ga_{0.47}As$ layer.**

***Index Terms*— Al_2O_3, capacitance, conductance, III–V, $In_{0.53}Ga_{0.47}As$, interface state defects, inversion, metal–oxide–semiconductor (MOS) system, minority carrier generation lifetime, oxide capacitance, semiconductor quality.**

Manuscript received July 16, 2014; revised September 7, 2014; accepted September 30, 2014. This work was supported in part by the Science Foundation Ireland under Project 09/IN.1/I2633, in part by the Components Research Division, Intel Corporation, Hillsboro, OR, USA, and in part by the European Commission through the Project entitled Compound Semiconductors for 3D Integration COMPOSE^3 under Grant FP7-ICT-2013-11-619325. The authors thank Dr. Brendan Sheehan of Tyndall National Institute, Cork, Ireland for development of the automated measurement system. The review of this paper was arranged by Editor R. Huang.

S. Monaghan, É. O'Connor, L. Floyd, K. Cherkaoui, I. M. Povey, and P. K. Hurley are with the Tyndall National Institute, University College Cork, Cork, Ireland (e-mail: scott.monaghan@tyndall.ie; eamon.oconnor@tyndall.ie; liam.floyd@tyndall.ie; karim.cherkaoui@tyndall.ie; ian.povey@tyndall.ie; paul.hurley@tyndall.ie).

R. Rios, F. Ferdousi, and K. J. Kuhn are with the Components Research, Intel Corporation, Hillsboro, OR 97124 USA (e-mail: rafael.rios@intel.com; fahmida.ferdousi@intel.com; kelin.ptd.kuhn@intel.com).

E. Ryan was with the Tyndall National Institute, University College Cork, Cork, Ireland. She is now with the Department of Mathematics, University College Cork, Cork, Ireland (e-mail: 111312041@umail.ucc.ie).

Color versions of one or more of the figures in this paper are available online at http://ieeexplore.ieee.org.

Digital Object Identifier 10.1109/TED.2014.2362524

I. Introduction: Context and Motivation

THE measurement and analysis of the metal-oxide-semiconductor (MOS) system has played a central role in the development of silicon-based complementary MOS (CMOS) technology over the past 50 years. The measurement of the capacitance (C) and conductance (G or G_m) of the MOS structure as a function of applied bias, alternating current (ac) signal frequency (ω), and temperature, allows for the determination of a wide range of properties such as the gate oxide capacitance, the semiconductor doping concentration, metal gate work functions, the density of interface states, and fixed charges in the oxide. The impedance-based analysis methods are described in [1] and [2].

To achieve an improvement in the energy efficiency of logic devices, there is currently a growing interest in exploring alternative semiconductors to silicon in either MOSFET [3]–[6] or tunnel FET [7]–[10] configurations. This has prompted research into applying the techniques proposed in [1] and [2], which were developed primarily for silicon-based MOS systems, to alternative semiconductors such as $In_{0.53}Ga_{0.47}As$ ($E_g \sim 0.75$ eV) and Ge ($E_g \sim 0.66$ eV) [11]–[27]. Considering the case of $In_{0.53}Ga_{0.47}As$-based MOS structures, there has been considerable progress in recent years in reducing the interface state density (D_{it}) [13], [17], [19], to the point where genuine surface inversion can be observed for both n- and p-type $In_{0.53}Ga_{0.47}As$ MOS capacitors [18]. Because of the reduced energy gap of $In_{0.53}Ga_{0.47}As$ ($\sim$0.75 eV) compared with silicon ($\sim$1.12 eV), it is possible to measure a minority carrier response of the $In_{0.53}Ga_{0.47}As$ MOS structure in inversion at room temperature and within the frequency range typical for impedance meters (20 Hz to 1 MHz) [18].

The objective of this paper is to report on an observed relationship between specific functions of the capacitance and conductance for the $In_{0.53}Ga_{0.47}As$ MOS system in inversion. During an investigation of the inversion behavior of the capacitance and conductance of the $In_{0.53}Ga_{0.47}As$ MOS system as a function of ac angular frequency (ω), the authors observe that the peak values of G_m/ω and $-dC/d\log_e(\omega)$ ($\equiv -\omega dC/d\omega$) are equal, and that these equal peak magnitudes occur at the same value of ω. This paper also demonstrates how this

relationship can be used to verify true inversion, and can be applied to extract the oxide capacitance and estimate the minority carrier generation lifetime.

The rest of this paper is structured in the following way.

1) Section II presents details of the $In_{0.53}Ga_{0.47}As$ MOS experimental samples, the observed capacitance–voltage (C–V) and G_m/ω–V experimental relationship, and the observation in inversion (at any given gate voltage) that G/ω and $-\omega dC/d\omega$ versus the angular frequency ω have an equal magnitude and this also occurs at the same angular frequency.
2) Section III describes the results of a physics-based ac simulation of the equivalent $In_{0.53}Ga_{0.47}As$ MOS system and shows that the experimentally observed relationship between G/ω and $-\omega dC/d\omega$ also results from the physics-based simulation of the ideal case.
3) Section IV provides a comparison of physics-based simulations of the ideal case to that of the experimental results, and it is demonstrated that through this approach the bulk minority carrier lifetime in the $In_{0.53}Ga_{0.47}As$ layer can be determined.
4) In Section V, by applying the equivalent circuit model for any MOS structure in inversion, the observed relationship of G/ω and $-\omega dC/d\omega$ is shown to be true, and hence confirmed generally true for any MOS structure in inversion. Further details are included in the Appendix.
5) In Section VI, the practical application of the observed relationship between G/ω and $-\omega dC/d\omega$ for the determination of the oxide capacitance (C_{ox}) is demonstrated, which can be especially challenging for thin oxides and alternative III–V MOS structures.
6) Section VII provides the Conclusion and the Appendix.

II. Experimental: Sample Details With C–V and G_m/ω–V Observations

The experimental results and analysis presented are for metal/Al_2O_3/$In_{0.53}Ga_{0.47}As$/InP MOS capacitors with both n- and p-doped $In_{0.53}Ga_{0.47}As$ epitaxial layers. $In_{0.53}Ga_{0.47}As$ epitaxial layers (2 μm) were grown by metal organic vapor phase epitaxy on InP (100) substrates. For the n-type samples, the $In_{0.53}Ga_{0.47}As$ layers were doped with sulphur to $\sim 4.4 \times 10^{17}$ cm^{-3} on heavily n-doped (S at $\sim 2 \times 10^{18}$ cm^{-3}) InP substrates. For the corresponding p-type samples, the $In_{0.53}Ga_{0.47}As$ layers were doped with zinc to $\sim 2.0 \times 10^{17}$ cm^{-3} on heavily p-doped (Zn at $\sim 3.3 \times 10^{18}$ cm^{-3}) InP substrates.

The focus of this paper is to report on the characteristic behavior of the capacitance and conductance in inversion, and to achieve inversion for an $In_{0.53}Ga_{0.47}As$-based MOS capacitor it is necessary to reduce D_{it} levels. Previous studies have shown that following an optimized $(NH_4)_2S$ surface preparation genuine inversion can be achieved in the $In_{0.53}Ga_{0.47}As$ MOS system [18], and this surface preparation approach is used for the experimental samples in this paper. The $In_{0.53}Ga_{0.47}As$ surfaces were initially degreased by sequentially rinsing for 1 min each in acetone, methanol, and isopropanol. Before the Al_2O_3 deposition, the samples were immersed in $(NH_4)_2S$ solution (10% in deionized H_2O) for 20 min at room temperature ($\sim$295 K). An $(NH_4)_2S$ concentration of 10% for 20 min at room temperature has been found to be the optimum in terms of suppressing the formation of $In_{0.53}Ga_{0.47}As$ native oxides, and in reducing the high-k/$In_{0.53}Ga_{0.47}As$ interface state density [12], [13]. The optimum 10% $(NH_4)_2S$ concentration has subsequently been confirmed to yield improvements in fully fabricated $In_{0.53}Ga_{0.47}As$ MOSFETs [28]. Following the 10% $(NH_4)_2S$ surface preparation, the transit time to the atomic layer deposition (ALD) chamber has been demonstrated to have a significant impact on the resulting interface state concentrations [12], [13]. The experimental results presented here are for a transfer time from the aqueous $(NH_4)_2S$ solution to the ALD chamber of $\sim$3 min. The Al_2O_3 dielectric, with a nominal thickness of 8 nm, was deposited by ALD at 300 °C using trimethyl aluminium (TMA) and H_2O. The first pulse in the ALD process was the TMA.

The gate metal contacts were formed by electron beam evaporation of Ni (70 nm) and Au (90 nm) by using a liftoff process. No back metal contacts were used to the InP substrate. The C–V and G_m/ω–V measurements were recorded using an E4980A Agilent LCR meter. The measurements presented were performed at 25 °C, on-wafer in a microchamber probe station (Cascade Microtech, model Summit 12971B) in a dry air (dew point < -65 °C) and dark environment.

Fig. 1(a), (b), (d), and (e) shows the C–V and G/ω–V response from 20 Hz to 1 MHz for the Al_2O_3/n-$In_{0.53}Ga_{0.47}As$ and Al_2O_3/p-$In_{0.53}Ga_{0.47}As$ MOS capacitors, showing the expected behavior for an inverted surface [18].

As shown in Fig. 1(a), the high-frequency capacitance at 1 MHz (for any gate bias < -2 V) reaches the expected high-frequency minimum capacitance based on the $In_{0.53}Ga_{0.47}As$ doping concentration. Fig. 1(d) shows a similar behavior for any gate bias $> \sim 1.5$ V. At low frequencies the capacitance tends toward C_{ox}. At intermediate frequencies, the value of the constant capacitance in inversion is limited by the minority carrier supply rate to the inversion region. It is important to emphasize that for gate voltages corresponding to strong inversion, interface states (D_{it}) cannot contribute to the minority carrier response, as all of the interface states are either empty (n-type $In_{0.53}Ga_{0.47}As$ in inversion) or fully occupied (p-type $In_{0.53}Ga_{0.47}As$ in inversion), and their occupancy does not change with the small ac modulation on the gate. In this case, the minority carriers generated in response to the small ac signal are supplied by generation of electron/hole pairs in the $In_{0.53}Ga_{0.47}As$ depletion region where the Fermi-level (E_f) crosses the intrinsic level (E_i), which is located away from the $In_{0.53}Ga_{0.47}As/Al_2O_3$ interface. At higher temperatures, minority carrier supply, based on diffusion of minority carriers (n_i^2/N) from the quasi-neutral region, also contributes to the minority carrier response [1, pp. 112–114].

For an inverted MOS structure, the transition frequency ($2\pi f_m = \omega_m$) is defined as the frequency at which the capacitance is midway between the lowest and highest capacitance measured in strong inversion. The transition frequency is highlighted as the magenta-colored curve as shown in Fig. 1(a) and occurs at a frequency (f_m) of 25 kHz.

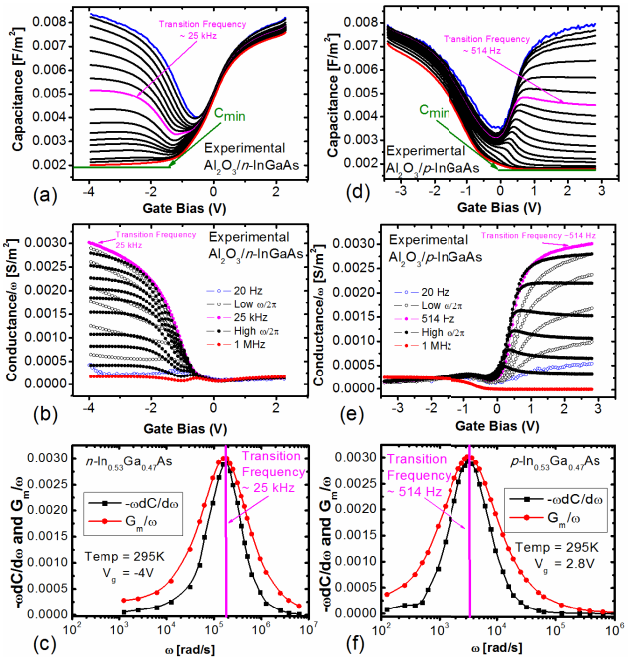

Fig. 1. (color online) Experimental measurements at room temperature of multifrequency (a) and (d) C–V responses, and (b) and (e) G_m/ω–V responses (the solid symbols are for frequencies $< \omega_m/2\pi$, and the open symbols are for frequencies $> \omega_m/2\pi$), from 20 Hz (blue) to the transition frequency (magenta) to 1 MHz (red) for n-type and p-type Al_2O_3(8 nm)/$In_{0.53}Ga_{0.47}As$/n^+-InP MOS structures with a Ni/Au gate, respectively. The experimentally extracted G_m/ω and $-\omega dC/d\omega$ are plotted as a function of the angular frequency (ω), for the n-type and p-type $In_{0.53}Ga_{0.47}As$ MOS systems in (c) and (f), respectively, at gate voltages corresponding to strong inversion ($V_g = -4$ V and $V_g = +2.8$ V, respectively). Moreover, the frequency at which the capacitance of (a) and (d) in the inversion region transcends from low frequency to high frequency, known as the transition frequency, corresponds to the frequency of the maximum value of G_m/ω in inversion, as demonstrated in (b) and (e), which is expected for true surface inversion behavior [1], [18]. The peak values of G_m/ω and $-\omega dC/d\omega$ for each type of doped semiconductor structure are both equal in magnitude and occur at the same angular frequency ω, as shown in (c) and (f) for n-type and p-type, respectively. The value of ω at which these peaks occur corresponds to the transition frequency, as identified in (a), (b), (d), and (e). The transition frequencies for the n-type and p-type MOS structures are ~25 kHz ($\times 2\pi$) and ~514 Hz ($\times 2\pi$), respectively.

Fig. 1(b) shows the corresponding G/ω–V response over the same frequency range, where the maximum value of G/ω corresponds to the same transition frequency as shown in Fig. 1(a), where $f_m = 25$ kHz. The Al_2O_3/p-$In_{0.53}Ga_{0.47}As$ MOS structure [Fig. 1(d) and (e)] also presents C–V and G/ω–V behavior similarly consistent with surface inversion, with a transition frequency (f_m) of 514 Hz.

It is evident from an inspection of the inversion regions as shown in Fig. 1(a), (b), (d), and (e) that G_m/ω has a maximum value around the frequency corresponding to the maximum rate of change of the capacitance with respect to frequency. As shown in Fig. 1(c) and (f), G_m/ω and $-dC/d\log_e(\omega)$ ($\equiv -\omega dC/d\omega$) are plotted versus ω, for the n-$In_{0.53}Ga_{0.47}As$ and p-$In_{0.53}Ga_{0.47}As$ MOS structures, respectively. The plots are presented for a gate bias corresponding to strong inversion at the Al_2O_3/$In_{0.53}Ga_{0.47}As$ interface (-4 V for the n-$In_{0.53}Ga_{0.47}As$ MOS structure and $+2.8$ V for the p-$In_{0.53}Ga_{0.47}As$ MOS structure).

As shown in Fig. 1(c) and (f), it is evident that the peak magnitudes of G_m/ω and $-\omega dC/d\omega$ are equal and that their peak values occur at the same angular frequency, which corresponds to the transition frequency (ω_m) of the n-type and p-type $In_{0.53}Ga_{0.47}As$ MOS structures.

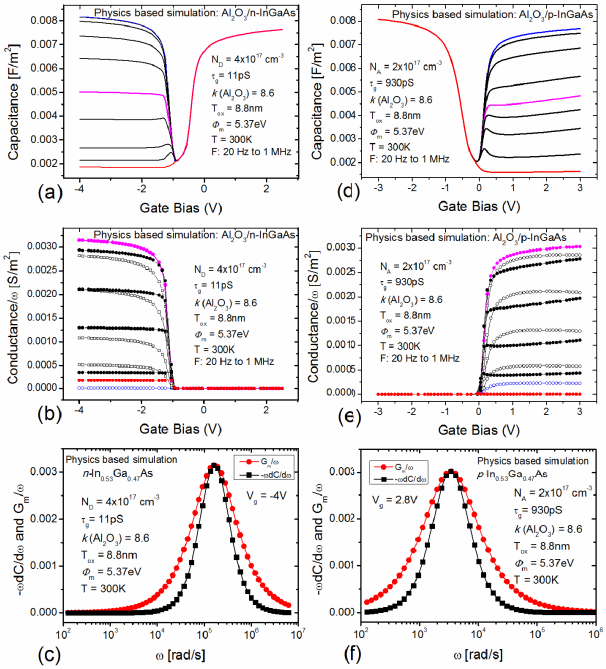

Fig. 2. (color online) Physics-based simulations at room temperature of multifrequency (a) and (d) C–V responses, and (b) and (e) G_m/ω–V responses (the solid symbols are for frequencies $< \omega_m/2\pi$, and the open symbols are for frequencies $> \omega_m/2\pi$), from 20 Hz (blue) to the transition frequency (magenta) to 1 MHz (red) for simulated n-type and p-type Al_2O_3(8 nm)/$In_{0.53}Ga_{0.47}As$/InP MOS structures, respectively. The simulated G_m/ω and $-\omega dC/d\omega$ are plotted as a function of the angular frequency (ω), for the simulated n-type and p-type $In_{0.53}Ga_{0.47}As$ MOS systems in (c) and (f), respectively, at gate voltages corresponding to strong inversion ($V_g = -4$ V and $V_g = +2.8$ V, respectively). The relevant simulation parameters are given throughout. The simulation is for the ideal case of no interface states, fixed charges, or border traps. The minority carrier generation lifetimes (τ_g) for the n-type and p-type $In_{0.53}Ga_{0.47}As$ depletion regions were adjusted to match the transition frequencies of ~25 kHz ($\times 2\pi$) and ~514 Hz ($\times 2\pi$) in the simulated peak values in (c) and (f), matching the experimental findings shown in Fig. 1, giving minority carrier generation lifetimes of 11 and 930 ps, respectively.

For other Al_2O_3/$In_{0.53}Ga_{0.47}As$ MOS structures in inversion which display different transition frequencies, we have observed (not shown) that these peak magnitudes of G_m/ω and $-\omega dC/d\omega$ are equal and occur at the transition frequency. These observations suggest that the relationship between G_m/ω and $-\omega dC/d\omega$ is general and not specific to the particular $In_{0.53}Ga_{0.47}As$ MOS structures examined. To explore this possibility, the relationship between G_m/ω and $-\omega dC/d\omega$ was investigated using physics-based simulations of Al_2O_3/$In_{0.53}Ga_{0.47}As$ MOS structures using a Synopsys Sentaurus Device Simulator, with the details in the following section.

III. Simulated C–V, G/ω–V, and Functional Responses in Inversion

Fig. 2 shows the simulated C–V and G_m/ω–V response from 20 Hz to 1 MHz for Al_2O_3/n-$In_{0.53}Ga_{0.47}As$/n^+InP [Fig. 2(a) and (b)] and Al_2O_3/p-$In_{0.53}Ga_{0.47}As$/p^+InP MOS capacitors [Fig. 2(d) and (e)]. The simulations assume the

ideal case of no interface states, no fixed charges, and no border traps in the $Al_2O_3/In_{0.53}Ga_{0.47}As/InP$ MOS structures. In the simulation, the minority carriers are provided by thermal generation of electron/hole pairs through deep levels (located near the midgap energy) in the $In_{0.53}Ga_{0.47}As$ depletion region, or by diffusion from the quasi-neutral bulk region. The minority carrier generation lifetime (τ_g) values used in the simulations are 11 ps for n-$In_{0.53}Ga_{0.47}As$ and 930 ps for p-$In_{0.53}Ga_{0.47}As$. At a temperature of 300 K, electron–hole pair generation in the depletion region is the dominant mechanism of minority carrier supply to the inversion region, and the minority carrier generation rate is $U = n_i/2\tau_g$ (where n_i is the $In_{0.53}Ga_{0.47}As$ intrinsic carrier concentration, taken as 6.3×10^{11} cm^{-3} [29]) [30], [31].

From the simulated C–V responses shown in Fig. 2(a) (n-type) and Fig. 2(d) (p-type), the capacitance is approximately constant as a function of the applied gate voltage in the regions of strong inversion of the $Al_2O_3/In_{0.53}Ga_{0.47}As$ interface. The corresponding simulated G/ω–V responses shown in Fig. 2(b) and (e) also indicate a constant G/ω value as a function of gate voltage in inversion. At given voltages in inversion, the value of G/ω peaks at values of ω occurring at the corresponding transition frequencies of the simulated C–V responses shown in Fig. 2(a) and (d). As shown in Fig. 2(c) and (f), the physics-based simulated G_m/ω and $-\omega dC/d\omega$ are plotted versus ω, and exhibit the same behavior as the experimental n-$In_{0.53}Ga_{0.47}As$ and p-$In_{0.53}Ga_{0.47}As$ MOS structures as shown in Fig. 1(c) and (f), respectively.

Comparing the plots shown in Fig. 1(a)–(f) and 2(a)–(f), respectively, we find a striking agreement. While the experimental C–V and G/ω–V responses shown in Fig. 1 are stretched out along the gate voltage axis due to the presence of interface states and the possible contribution of traps in the Al_2O_3 close to the Al_2O_3/n-$In_{0.53}Ga_{0.47}As$ interface [21], the salient features associated with the expected multifrequency C–V and G/ω–V response for an inverted surface are observed in the experimental data. The experimental and simulated G_m/ω and $-\omega dC/d\omega$ versus ω exhibit peaks at the same frequency and with the same magnitude.[1] The simulated full width half maximum of $-\omega dC/d\omega$ is less than that for G_m/ω, as observed in the experimental characteristics. The same behavior of G_m/ω and $-\omega dC/d\omega$ is also noted for simulations of silicon MOS structures (not shown), where the value of (ω_m) is shifted to lower frequencies (<1 Hz) than exhibited by $In_{0.53}Ga_{0.47}As$, due to the generally higher values of minority carrier lifetime in silicon (typically in the 100 μs to 1 ms range for device grade silicon [32]).

[1]It is noted from simulations that G/ω and $-dC/d\log_e(\omega)$ ($\equiv -\omega\, dC/d\omega$) also exhibit peak values in the accumulation region of the C–V response (at very high frequencies in the GHz range), and in the case of a D_{it} response in the gate bias range of the C–V response corresponding to depletion. The peak values of $-\omega dC/d\omega$ and G/ω in accumulation, and of $-\omega dC/d\omega$ and G/ω in depletion (with D_{it}), do not have the same magnitudes or ω_m dependencies as the strong inversion case and are not discussed further in this paper.

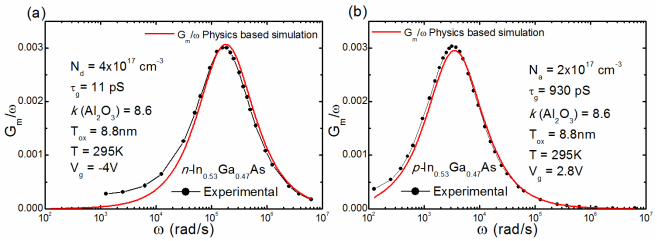

Fig. 3. (color online) Measured (black line and filled circles) and simulated (solid red line) G_m/ω plotted as a function of the angular frequency (ω). (a) For Al_2O_3(8 nm)/n-$In_{0.53}Ga_{0.47}As$/InP MOS structure in strong inversion for a gate voltage of $V_g = -4$ V. (b) For Al_2O_3(8 nm)/p−$In_{0.53}Ga_{0.47}As$/InP MOS structure in strong inversion for a gate voltage of $V_g = +2.8$ V. The simulations are for the ideal case of no interface states, fixed charges, or border traps. The relevant simulation parameters are shown. There is a good agreement between the measured and simulated plots over a wide range of ac frequency, demonstrating that interface states and/or border traps are playing a negligible role in the measured conductance at these gate voltages in strong inversion.

IV. Comparison of Physics-Based Simulation and Experimental G/ω–ω Responses in Inversion

Fig. 3(a) and (b) shows the measured and physics-based simulated G/ω versus ω for the Al_2O_3/n-$In_{0.53}Ga_{0.47}As/n^+InP$ and Al_2O_3/p-$In_{0.53}Ga_{0.47}As/p^+InP$ MOS capacitor structures, respectively. There is very good agreement in the form of the measured and simulated G/ω over a wide range of ac frequency, demonstrating that interface states and/or border traps are playing very little role in the measured conductance at the gate voltages selected in strong inversion (−4 V for n-$In_{0.53}Ga_{0.47}As$ and +2.8 V for p-$In_{0.53}Ga_{0.47}As$). The measured and simulated $-\omega dC/d\omega$ characteristics are also in very good agreement for both the Al_2O_3/n-$In_{0.53}Ga_{0.47}As/n^+InP$ and Al_2O_3/p-$In_{0.53}Ga_{0.47}As/p^+InP$ structures (not shown).

The values used in the physics-based simulations are shown in Fig. 3. These compare well with the nominal experimental values. The value of $k = 8.6$ for the ALD deposited Al_2O_3 was evaluated from an Al_2O_3 thickness series on n-$In_{0.53}Ga_{0.47}As$ [33], [34]. The alignment of the simulated peak angular frequencies with the experimental values (ω_m) is achieved by altering the simulated minority carrier generation lifetime (τ_g) in the $In_{0.53}Ga_{0.47}As$ layer. The minority carrier generation lifetime determines the minority carrier generation rate ($U = n_i/2\tau_g$), where n_i is the intrinsic carrier concentration in the $In_{0.53}Ga_{0.47}As$.

The values of τ_g required in the simulations to match the experimental peak angular frequencies are 11 ps for the n-type $In_{0.53}Ga_{0.47}As$ and 930 ps for the p-type $In_{0.53}Ga_{0.47}As$. The difference in the (τ_g) values for the n- and p-type $In_{0.53}Ga_{0.47}As$ reflects the difference in the values of ω_m for the two samples. This τ_g value of 930 ps obtained for the p-type $In_{0.53}Ga_{0.47}As$ (2×10^{17} cm^{-3}, Zn) compares well with values reported in [35]. The value of 11 ps obtained for the n-type $In_{0.53}Ga_{0.47}As$ (4×10^{17} cm^{-3}, S) is lower than reported in [36]. However, a difference in τ_g values to previous literature reports is not unexpected as τ_g values are strongly dependent on the density and capture cross section values of defects which align with the midgap energy in the semiconductor, and τ_g values spanning the range 20 μs

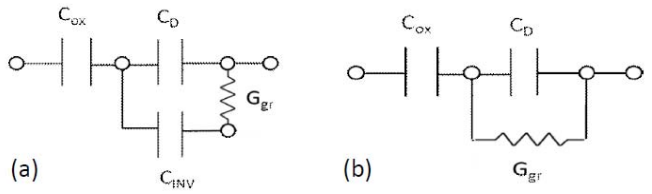

Fig. 4. (a) Equivalent circuit model for the MOS system in inversion, based on the maximum depletion capacitance (C_D) in series with the inversion layer capacitance ($C_{\rm INV}$). The provision of minority carriers to the inversion layer is modeled by a generation/recombination conductance ($G_{\rm gr}$). (b) Equivalent circuit model for the case of strong inversion where $\omega C_{\rm INV} \gg G_{\rm gr}$. Following [1, p. 118, Fig. 4.5(d) and (e)] for (a) and (b), respectively.

to 25 ps have been reported for $In_{0.53}Ga_{0.47}As$ with doping concentrations from $\sim 1 \times 10^{14}$ to $\sim 2 \times 10^{19}$ cm^{-3} [36].

It is noted that based on the temperature dependence of the conductance in inversion (not shown), the activation energies for the experimental n- and p-type $In_{0.53}Ga_{0.47}As$ MOS samples examined in this paper are 0.31 eV (n-$In_{0.53}Ga_{0.47}As$) and 0.37 eV (p-$In_{0.53}Ga_{0.47}As$) for temperatures less than 140 °C [18], indicating that generation of electron hole pairs through midgap states in the $In_{0.53}Ga_{0.47}As$ depletion region is the dominant mechanism of minority carrier supply in the experimental samples examined in this paper.

V. Equivalent Circuit Inversion Model and the Mathematical Derivation of G/ω and $-\omega {\rm d}C/{\rm d}\omega$

The observations from experimentation and from physics-based simulations that G/ω and $-{\rm d}C/{\rm dlog}_e(\omega)$ ($\equiv -\omega {\rm d}C/{\rm d}\omega$) have peak values at the same frequencies and that the peak values have the same magnitudes suggest that the relationship is generally true for the MOS system in inversion. Therefore, it should be possible to derive this relationship based on the equivalent circuit model for the MOS system in inversion. An equivalent circuit model was proposed by Nicollian and Brews [1, p. 118, Fig. 4.5(d) and (e); see also pp. 115–148] for the MOS system in inversion based on capacitance and conductance elements.

Fig. 4(a) shows the equivalent circuit for the MOS system in inversion, comprising the inversion layer capacitance ($C_{\rm INV}$) in series with a frequency dependent conductance ($G_{\rm gr}(\omega)$) that represents the supply of minority carriers to the inversion layer through generation and recombination. This series combination of $G_{\rm gr}(\omega)$ and $C_{\rm INV}$ appears in parallel with the depletion capacitance (C_D), and finally this parallel combination is in series with the oxide capacitance ($C_{\rm ox}$).

As the MOS structure is driven further into inversion, $C_{\rm INV}$ increases exponentially with the oxide/semiconductor surface potential. In the condition where $\omega C_{\rm INV} \gg G_{\rm gr}(\omega)$, the equivalent circuit shown in Fig. 4(a) reduces to that shown in Fig. 4(b). The remainder of this analysis deals with the circuit model condition shown in Fig. 4(b), but it can be easily shown[2] that as $C_{\rm INV}$ tends toward infinity the equivalent circuit model as shown in Fig. 4(a) approaches the model as shown in Fig. 4(b). For the circuit model as shown Fig. 4(b), the C and G/ω terms of the total circuit impedance are given by

$$C = C_{\rm ox}\left[1 - \frac{\omega^2 C_{\rm ox}(C_{\rm ox}+C_D)}{(G_{\rm gr}(\omega))^2 + \omega^2(C_{\rm ox}+C_D)^2}\right] \quad (1)$$

$$G/\omega = G_{\rm gr}(\omega)\frac{\omega C_{\rm ox}^2}{(G_{\rm gr}(\omega))^2 + \omega^2(C_{\rm ox}+C_D)^2}. \quad (2)$$

Equations (1) and (2) provide a potential route to investigate whether the relationship between G/ω and $-\omega {\rm d}C/{\rm d}\omega$ observed through experiments and physics-based simulations can be shown mathematically to be true in all cases. As a first step, it is important to first check that the equivalent circuit model as shown in Fig. 4(b) provides an accurate description of the MOS system in inversion. To check this, the equivalent circuit model predications for G/ω and $-\omega {\rm d}C/{\rm d}\omega$ are compared with the case of strong inversion obtained from the physics-based simulations. The results are shown in Fig. 5 and indicate that the equivalent circuit model is in excellent agreement with the physics-based simulations over the full angular frequency range of ω. For the equivalent circuit model, the parameters entered in are C_D, $C_{\rm OX}$, ω, and ω_m to give $G_{\rm gr}(\omega) = \omega_m(C_{\rm ox}+C_D)$ (1). For the physics-based simulations, the parameters entered in are the same as those shown in Fig. 3. It is demonstrated in Fig. 5 that by matching only the transition frequency (ω_m) through its relationship to τ_g, the physics-based simulations and the equivalent circuit model mathematical derivations provide excellent agreement. Given the simplicity of the equivalent circuit model, we therefore investigate the mathematical relationship between G/ω and $-\omega {\rm d}C/{\rm d}\omega$ using (1) and (2).

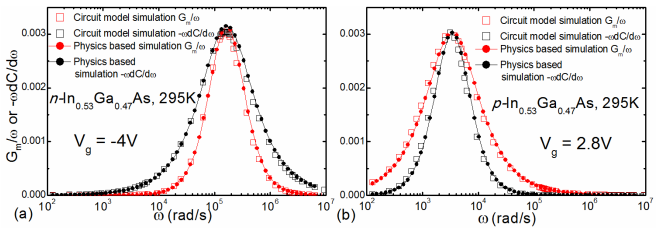

Fig. 5. (color online) Comparison for G/ω (red) and $-\omega {\rm d}C/{\rm d}\omega$ (black) derived from the equivalent circuit models of (1) and (2) (open squares), and the physics-based simulations (closed circles). (a) For Al_2O_3(8 nm)/n-$In_{0.53}Ga_{0.47}As$. (b) For Al_2O_3(8 nm)/p-$In_{0.53}Ga_{0.47}As$ MOS structures in inversion. For the physics-based simulations, the parameters used are those used for Fig. 3. For the equivalent circuit model, the parameters entered into the model are the oxide capacitance ($C_{\rm ox}$), the maximum depletion capacitance in inversion (C_D), ω, and ω_m to give $G_{\rm gr}(\omega) = \omega_m(C_{\rm ox}+C_D)$ [1].

The Appendix shows that, regardless of the dependence of the unknown function $G_{\rm gr}(\omega)$ on ω, G/ω will exhibit a maximum value when $\omega = \omega_m$, and this maximum value is given by

$$[G/\omega]_{\rm max} = \frac{C_{\rm ox}^2}{2(C_{\rm ox}+C_D)}. \quad (3)$$

Also, at $\omega = \omega_m$, $G_{\rm gr}(\omega)$ must satisfy the condition

$$G_{\rm gr}(\omega_m) = \omega_m(C_{\rm ox}+C_D). \quad (4)$$

Furthermore, provided that the derivatives of $G_{\rm gr}(\omega)$ are zero at ω_m, the graph of $-\omega {\rm d}C/{\rm d}\omega$ will also have a local

[2]We have derived, but not included (due to page length constraints), the circuit model as shown in Fig. 4(a) for C, G, G_m/ω, and $-\omega {\rm d}C/{\rm d}\omega$, and determined the minimum inversion capacitance values that agree with our experimental results at the inversion gate voltages selected, which indicate that a strong inversion is achieved.

maximum at the same angular frequency $\omega = \omega_m$, and the value of this maximum is

$$[-\omega \mathrm{d}C/\mathrm{d}\omega]_{\max} = \frac{C_{\mathrm{ox}}^2}{2(C_{\mathrm{ox}} + C_D)}. \quad (5)$$

Equations (3) and (5) lead to the same peak value magnitudes for both expressions, so based on the equivalent circuit as shown in Fig. 4(b), the experimental and simulated relationship between G/ω and $-\omega \mathrm{d}C/\mathrm{d}\omega$ can be demonstrated mathematically based on selected conditions on the function $G_{\mathrm{gr}}(\omega)$. The Appendix shows that, for the case of $G_{\mathrm{gr}}(\omega)$ having a constant value, the Kramers–Kronig relations [37], [38] hold between the real (G/ω) and imaginary $(-\omega \mathrm{d}C/\mathrm{d}\omega)$ parts of the overall impedance. In this case, G/ω and $-\omega \mathrm{d}C/\mathrm{d}\omega$ are related at all angular frequencies, as presented in this paper. This agrees with [1, p. 198] for any circuit made up solely of passive elements.

Finally, the equivalent circuit model (and by inference the experimental data and the physics-based simulations) predict that the magnitudes of the peaks in both functions are uniquely related only via the oxide capacitance and the maximum depletion capacitance in inversion, which leads us to a new and simple method of determining the oxide capacitance of MOS-based devices, which is considered in the following section.

VI. Practical Application of the G/ω and $-\omega \mathrm{d}C/\mathrm{d}\omega$ Relationship in the Evaluation of C_{OX}

It can be a challenge to accurately determine C_{ox} in narrow band gap III–V-based MOS systems due to the effects of interface states and traps in the gate oxide, combined with the low density of states in the III–V conduction band. The effect is compounded for thin oxides with high leakage currents over the bias range of the C–V response, when low-frequency noise can also be a complicating factor. Indeed, it is also generally a challenge for the case of silicon-based MOS systems when the equivalent oxide thickness is around 1.5 nm or below owing to the effect of oxide leakage on the C–V response [39], which affects both quasi-static C–V measurements over the full bias range and ac-based impedance measurements in accumulation.

The consequence of the equality between (3) and (5), that the maximum peak values of G/ω and $-\omega \mathrm{d}C/\mathrm{d}\omega$ are equal, is that an alternative approach is possible to determine C_{ox} based on multifrequency C–V and G–V measurements. Moreover, the measurements are performed with the MOS system biased in the condition of inversion. This has advantages for samples where oxide leakage is an issue in strong accumulation, or in III–V-based MOS devices where establishing the value of C_{ox} from $C_{\max}$ can be complicated because of the presence of accumulation frequency dispersion, D_{it} in the conduction band, and/or the low conduction band density of states [13], [15].

For the experimental samples examined in this paper, the oxide thickness values have been determined by transmission electron microscopy (TEM) analysis; the dielectric constant of the ALD-deposited Al_2O_3 has been evaluated from an Al_2O_3 thickness series as 8.6 [33], [34], and the doping concentrations in the $In_{0.53}Ga_{0.47}As$ layers are known from the growth process and semiconductor characterization methods. As a consequence, the samples provide a good test to assess whether the predications of (3) and (5) are in line with the experimental observations. Fig. 6 shows the experimental values of G_m/ω and $-\omega \mathrm{d}C/\mathrm{d}\omega$ plotted for both the n- and p-type $In_{0.53}Ga_{0.47}As$ MOS structures in inversion. The gray shaded area is the expected peak value range based on a theoretical oxide capacitance range calculated from an Al_2O_3 thickness in the range 8–9 nm (from TEM) and a relative permittivity value of 8.6. As can be seen from Fig. 6, the actual peak values of G_m/ω and $-\omega \mathrm{d}C/\mathrm{d}\omega$ are within the expected range of C_{ox} and can be measured precisely in this range by using $C_{\mathrm{ox}}^2/(2(C_{\mathrm{ox}} + C_D))$ from (3) and (5), illustrating the usefulness for extracting C_{ox} for the MOS system in inversion.[3]

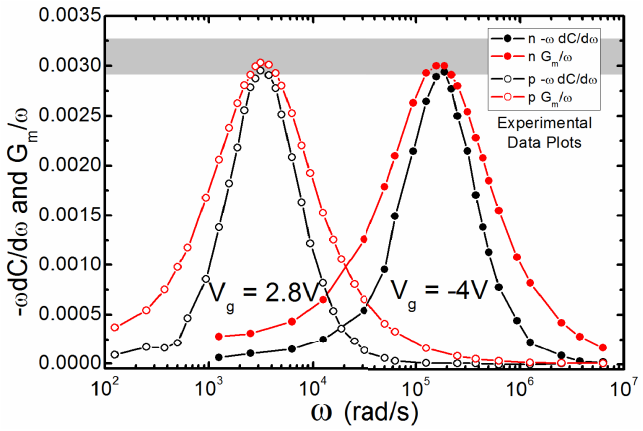

Fig. 6. (color online) Experimental data plots of G_m/ω and $-\omega \mathrm{d}C/\mathrm{d}\omega$ for both the n- and p-type $In_{0.53}Ga_{0.47}As$ MOS structures as shown in Fig. 1. Gray shaded area: expected peak value range based on a theoretical oxide capacitance range calculated from an Al_2O_3 thickness in the range 8–9 nm (from TEM) and a relative permittivity value of 8.6 [33], [34]. The maximum peak values of G_m/ω and $-\omega \mathrm{d}C/\mathrm{d}\omega$ can be measured precisely in this range using $C_{\mathrm{ox}}^2/(2(C_{\mathrm{ox}} + C_D))$ from (3) and (5), and illustrating the usefulness for extracting C_{ox}.

A further relevant observation is that the functions G_m/ω and $-\omega \mathrm{d}C/\mathrm{d}\omega$ exhibit symmetry about ω_m when plotted on a logarithmic ω axis. This implies that the function $G_{\mathrm{gr}}(\omega)$ also has a mathematical symmetry about ω_m.

The function $G_{\mathrm{gr}}(\omega)$ can be extracted directly from the experimental data [using (1) and (2), see the Appendix] and from the required symmetry in $G_{\mathrm{gr}}(\omega)$ around ω_m. There is also a third condition from (4), that at ω_m the following relationship holds, $G_{\mathrm{gr}}(\omega) = \omega_m(C_{\mathrm{ox}} + C_D)$. These three conditions can be used to obtain a more accurate evaluation of C_{ox}. This is shown in Fig. 7 for the Al_2O_3/n-$In_{0.53}Ga_{0.47}As$/n^+InP sample.

The method to extract and refine the accuracy of C_{ox} as shown in Fig. 7 is as follows: from the experimental results the value of ω_m is known (solid black vertical line

[3] As the MOS structure is driven further into inversion with the applied gate voltage, more accurate peak values are obtained and so more accurate C_{ox} extractions are achieved. Hence, for practical MOS systems, the measurements could be performed at reasonably low inversion gate voltages, before gate oxide leakage influences the data, and then extrapolated to gate voltages further into inversion.

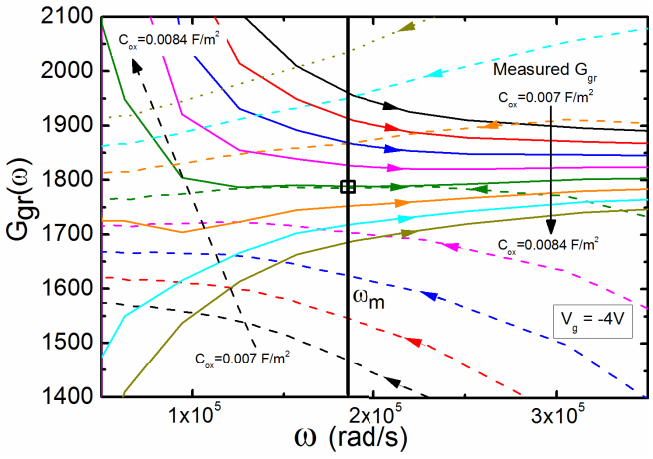

Fig. 7. (color online) Plot of the function $G_{\rm gr}(\omega)$ versus ω for the Al_2O_3/n-$In_{0.53}Ga_{0.47}As$/n^+InP MOS device for a range of $C_{\rm ox}$ values. The values of $G_{\rm gr}(\omega)$ obtained from the experimental results are shown as solid lines and derived from the expression for $G_{\rm gr}(\omega) = G(\omega)(C_{\rm ox} + C_D)/(C_{\rm ox} - C(\omega))$ (see the Appendix). Dotted lines: values of $G_{\rm gr}(\omega)$ which are required from the symmetry condition. Solid black vertical line: experimentally determined value of ω_m. Black box: value of $G_{\rm gr}(\omega)$ at ω_m which is equal to $\omega_m(C_{\rm ox}+C_D)$, and is shown for the case when all three conditions for $G_{\rm gr}(\omega)$ coincide at ω_m. An accurate value is obtained for $C_{\rm ox}$ when all of the three functions coincide, which in this case corresponds to $C_{\rm ox} = 0.0078$ F/m^2. The data shown is for $V_g = -4$ V (the equivalent treatment for the p-type sample is analogous, giving $C_{\rm ox} \sim 0.0077$ F/m^2 when $V_g = +2.8$ V).

shown in Fig. 7). A value of $C_{\rm ox}$ is then selected (with C_D calculated independently), and $G_{\rm gr}(\omega)$ is determined ($G_{\rm gr}(\omega) = \omega_m(C_{\rm ox} + C_D)$), which will represent a point on the line drawn at ω_m. $G_{\rm gr}(\omega)$ can also be determined across the full frequency range from the experimental results, using the same $C_{\rm ox}$ value. With this value of $C_{\rm ox}$, a corresponding $G_{\rm gr}(\omega)$ can be evaluated from the requirements of symmetry (see the Appendix). The correct value of $C_{\rm ox}$ is obtained when these three values of $G_{\rm gr}(\omega)$ coincide at ω_m. This is shown in Fig. 7. The plots are shown for changes in $C_{\rm ox}$ in increments of 0.0002 F/m^2, and the approach can be clearly seen to be very sensitive to changes in $C_{\rm ox}$. When all three conditions coincide at ω_m, we achieve a value of $C_{\rm ox} \sim 0.0078$ F/m^2. As shown in Fig. 7, when the correct value of $C_{\rm ox}$ is selected, the values of $G_{\rm gr}(\omega)$ derived from the experimental results, and those obtained from symmetry, become approximately constant about ω_m, which is the requirement for the two functions G/ω and $-\omega {\rm d}C/{\rm d}\omega$ to have coinciding local maxima at ω_m. The same approach also works for the Al_2O_3/p-$In_{0.53}Ga_{0.47}As$/p^+InP sample (not shown) and yields a $C_{\rm ox} \sim 0.0077$ F/m^2.

VII. Conclusion

Experimental measurements for the n-type and p-type $In_{0.53}Ga_{0.47}As$ MOS system demonstrate a unique relationship between particular functions of the capacitance (C) and conductance (G or G_m) in inversion versus the ac signal angular frequency (ω), where the maximum peak value of the function G/ω is equal to the maximum peak value of the function $-{\rm d}C/{\rm dlog}_e(\omega)$ ($\equiv -\omega {\rm d}C/{\rm d}\omega$). Moreover, these maximum peak values occur at the same angular frequency ($\omega = \omega_m$). The experimental observation has been confirmed by physics-based ac simulations of the $In_{0.53}Ga_{0.47}As$ MOS system, showing that the equality holds for the case of inversion. It has also been demonstrated that the relationship between G/ω and $-\omega {\rm d}C/{\rm d}\omega$ can be derived based on the equivalent circuit for the MOS system in inversion, and that the equality between G/ω and $-\omega {\rm d}C/{\rm d}\omega$ at the transition frequency ($\omega = \omega_m$) is generally true for any MOS system in inversion provided certain conditions on the minority carrier generation and recombination conductance function ($G_{\rm gr}(\omega)$) apply.

This relationship between G/ω and $-\omega {\rm d}C/{\rm d}\omega$ at $\omega = \omega_m$ provides a new approach to distinguish between genuine surface inversion and high interface state defect density values in narrow band gap MOS structures. In addition, the location of ω_m, in conjunction with physics-based ac simulations, yields the minority carrier generation lifetime (τ_g) in the $In_{0.53}Ga_{0.47}As$ layer, which could be helpful in evaluating the quality of the semiconductor crystal, and to predict the expected minimum OFF-state current in MOSFETs [40], [41]. Furthermore, as the peak values of the two functions G/ω and $-\omega {\rm d}C/{\rm d}\omega$ at $\omega = \omega_m$ are equal to $C_{\rm ox}^2/(2(C_{\rm ox} + C_D))$, where $C_{\rm ox}$ is the oxide capacitance per unit area and C_D is the semiconductor depletion capacitance in strong inversion, the method can be used to extract the oxide capacitance of the MOS system in inversion. In addition, the low- and high-frequency symmetry could be used to filter out the effects of low-frequency noise. Finally, as the measurements are made in inversion, it could be less sensitive to oxide leakage and to the effect of frequency dispersion in accumulation, which are typically reported for narrow band gap III–V MOS systems. Hence, the method could potentially be applied to any MOS system regardless of the materials used, device architecture or technology node scaling level.

Appendix

We have observed experimentally that the graphs of $f_1(\omega) = G(\omega)/\omega$ and $f_2(\omega) = -\omega {\rm d}C(\omega)/{\rm d}\omega$ both have the same local maximum value at the same value of ω. They also both exhibit a very clear graphical symmetry when plotted against the logarithm of ω (regardless of the logarithmic scale, say x).

We defined ω_m for any MOS system to be the angular frequency at which the decreasing capacitance $C(\omega)$ is midway between its low-frequency limit ($C_{\rm ox}$) and its high-frequency limit $C_DC_{\rm ox}/(C_D+C_{\rm ox})$, that is, $C_{\rm mid} = 0.5(C_{\rm ox} + (C_D.C_{\rm ox}/(C_D + C_{\rm ox})))$. Because $(1) = C_{\rm mid}$ at ω_m, then equating and solving for $G_{\rm gr}(\omega_m)$ we find that the unknown function $G_{\rm gr}(\omega)$ must satisfy $G_{\rm gr}(\omega) = \omega_m(C_D + C_{\rm ox})$ when $\omega = \omega_m$.

Therefore, $f_1'(\omega_m) = 0$. Differentiating once again gives $f_1''(\omega_m) < 0$, thus $f_1(\omega)$ has a local maximum at $\omega = \omega_m$, and the value of this local maximum is $f_1(\omega_m) = C_{\rm ox}^2/(2(C_D + C_{\rm ox}))$. A further calculation shows that $f_1(\omega_m)(1 - (G_{\rm gr}'(\omega_m)/(C_D + C_{\rm ox}))) = f_2(\omega_m)$. Hence, the two functions will cross at $\omega = \omega_m$ only if $G_{\rm gr}'(\omega_m) = 0$, hence this is a requirement on $G_{\rm gr}(\omega)$.

Although it cannot be demonstrated using higher order derivatives that $f_2(\omega)$ has a local maxima at ω_m, it is possible

to demonstrate that $f_2(\omega)$ has a local maxima by using the symmetry about ω_m which is evident in the experimental and simulated functions $f_1(\omega)$ and $f_2(\omega)$ (Figs. 1–3, 5, and 6).

It can easily be shown that any function $f(\omega)$ that exhibits graphical symmetry about $\omega = \omega_m$ in a plot of $f(\omega)$ versus any logarithmic scale x of ω necessarily has the mathematical symmetry $f(\omega) = f(\omega_m^2/\omega)$. Since $f_1(\omega) = G(\omega)/\omega$ exhibits graphical symmetry about $\omega = \omega_m$ when plotted against $\mathrm{Log}_x(\omega)$, we must therefore have $f_1(\omega) = f_1(\omega_m^2/\omega)$ satisfied. This can only happen if $G_{\mathrm{gr}}(\omega)$ has the mathematical symmetry

$$G_{\mathrm{gr}}\left(\frac{\omega_m^2}{\omega}\right) = \frac{(C_{\mathrm{ox}} + C_D)^2\omega_m^2}{G_{\mathrm{gr}}(\omega)}. \tag{6}$$

We observe that the preceding relationship returns our earlier expression of $G_{\mathrm{gr}}(\omega) = \omega_m(C_D + C_{\mathrm{ox}})$ when $\omega = \omega_m$ as required. Differentiating (6) twice across with respect to ω and setting $\omega = \omega_m$ immediately gives us the requirement that $G''_{\mathrm{gr}}(\omega) = 0$.

Although $G_{\mathrm{gr}}(\omega)$ is not a constant function, it does appear constant about $\omega = \omega_m$ and belongs to a large family of so-called flat functions. This property of the $G_{\mathrm{gr}}(\omega)$ function ensures $G_{\mathrm{gr}}(\omega)$ has the symmetry in (6) about $\omega = \omega_m$, and that all derivatives of all orders are zero at $\omega = \omega_m$, consequentially ensuring that $f_1(\omega)$ and $f_2(\omega)$ exhibit graphical symmetry as observed when plotted against $\log_x(\omega)$ and will have the same local maxima at $\omega = \omega_m$ as also observed.

From (1) and (2) it follows that $G_{\mathrm{gr}}(\omega) = G(\omega)(C_{\mathrm{ox}}+C_D)/(C_{\mathrm{ox}} - C(\omega))$. Consequently, Fig. 7 shows plotting $G_{\mathrm{gr}}(\omega)$ using this expression, the symmetry expression of (6), and $G_{\mathrm{gr}}(\omega) = \omega_m(C_D+C_{\mathrm{ox}})$ when $\omega = \omega_m$. When $G_{\mathrm{gr}}(\omega)$ has this constant value about $\omega = \omega_m$, the Kramers–Kronig relations hold. For a linear causal time-invariant system which in the angular frequency domain is represented by $r(\omega) = g(\omega)i(\omega)$, with $i(\omega)$ being the input and $r(\omega)$ being the output response, then the real and imaginary parts of the measured quantity $g(\omega) = g_R(\omega) + ig_I(\omega)$ are related by

$$g_R(\omega) = \frac{-2}{\pi}\mathrm{P}\int_0^\infty \frac{xg_I(x)}{x^2-\omega^2}dx \tag{7a}$$

$$g_I(\omega) = \frac{2\omega}{\pi}\mathrm{P}\int_0^\infty \frac{g_R(x)}{x^2-\omega^2}dx. \tag{7b}$$

If $G_{\mathrm{gr}}(\omega)$ is a constant about $\omega = \omega_m$ and taking $g_R(\omega) = G(\omega)/\omega^2$ and $\mathrm{g}_I(\omega) = (C(\omega) - C_{\mathrm{ox}})/\omega$, (7a) and (7b) give

$$\frac{G(\omega)}{\omega^2} = \frac{-2}{\pi}\mathrm{P}\int_0^\infty \left(\frac{x}{x^2-\omega^2}\right)\left(\frac{C(x)-C_{\mathrm{ox}}}{x}\right)dx. \tag{8}$$

Because $\mathrm{P}\int_0^\infty (1/(x^2-\omega^2))dx = 0$ then $f_1(\omega)$ and $f_2(\omega)$ will intersect when $(dC(\omega)/d\omega) = (-G(\omega)/\omega^2) = (2/\pi)\,\mathrm{P}\int_0^\infty ((C(x)/(x^2-\omega^2)))dx$. This leads to our functions crossing at $\omega = G_{\mathrm{gr}}/(C_D + C_{\mathrm{ox}})$, that is, at $\omega = \omega_m$ as before. We also have $((C(\omega) - C_{\mathrm{ox}})/\omega) = (2\omega/\pi)\mathrm{P}\int_0^\infty (G(x)/(x^2(x^2-\omega^2)))dx$ so that $C(\omega) - C_{\mathrm{ox}} = (2\omega^2/\pi)\mathrm{P}\int_0^\infty ((1/x^2)(G(x)/(x^2-\omega^2)))dx$. Differentiating across with respect to ω and calculating $\omega\mathrm{d}C(\omega)/\mathrm{d}\omega$ quickly gives

$$f_1(\omega) - f_2(\omega) = \frac{\omega\omega_m C_{\mathrm{ox}}^2(\omega-\omega_m)^2}{(C_{\mathrm{ox}}+C_D)(\omega^2+\omega_m^2)^2}. \tag{9}$$

Equation [9] explicitly shows the relationship between our two functions $f_1(\omega)$ and $f_2(\omega)$ for a constant $G_{\mathrm{gr}}(\omega)$. Also note that $f_1(\omega)$ and $f_2(\omega)$ are equal in (9) for $\omega = \omega_m$, as observed.

REFERENCES

[1] E. H. Nicollian and J. R. Brews, *MOS Physics and Technology*. New York, NY, USA: Wiley, 1982

[2] E. H. Nicollian and A. Goetzberger, "The Si-SiO_2 interface—Electrical properties as determined by the metal-insulator-silicon conductance technique," *Bell Syst. Tech. J.*, vol. 46, no. 6, pp. 1055–1133, 1967.

[3] M. Radosavljevic *et al.*, "Advanced high-K gate dielectric for high-performance short-channel $In_{0.7}Ga_{0.3}As$ quantum well field effect transistors on silicon substrate for low power logic applications," in *Proc. IEEE Int. Electron Devices Meeting*, Dec. 2009, pp. 1–4.

[4] S. J. Bentley *et al.*, "Electron mobility in surface- and buried-channel flatband $In_{0.53}$ $Ga_{0.47}As$ MOSFETs with ALD Al_2O_3 gate dielectric," *IEEE Electron Device Lett.*, vol. 32, no. 4, pp. 494–496, Apr. 2011.

[5] M. Yokoyama *et al.*, "Sub-10-nm extremely thin body InGaAs-on-insulator MOSFETs on Si wafers with ultrathin Al_2 O_3 buried oxide layers," *IEEE Electron Device Lett.*, vol. 32, no. 9, pp. 1281–1220, Sep. 2011.

[6] K. J. Kuhn, "Considerations for ultimate CMOS scaling," *IEEE Trans. Electron Devices*, vol. 59, no. 7, pp. 1813–1828, Jul. 2012.

[7] H. Zhao, Y. Chen, Y. Wang, F. Zhou, F. Xue, and J. Lee, "InGaAs tunneling field-effect-transistors with atomic-layer-deposited gate oxides," *IEEE Trans. Electron Devices*, vol. 58, no. 9, pp. 2990–2995, Sep. 2011.

[8] Q. Zhang, S. Sutar, T. Kosel, and A. Seabaugh, "Fully-depleted Ge interband tunnel transistor: Modeling and junction formation," *Solid-State Electron.*, vol. 53, no. 1, pp. 30–35, 2009.

[9] A. C. Seabaugh and Q. Zhang, "Low-voltage tunnel transistors for beyond CMOS logic," *Proc. IEEE*, vol. 98, no. 12, pp. 2095–2110, Dec. 2010.

[10] G. Dewey *et al.*, "Fabrication, characterization, and physics of III–V heterojunction tunneling field effect transistors (H-TFET) for steep subthreshold swing," in *Proc. IEEE IEDM*, Dec. 2011, pp. 33.6.1–33.6.4.

[11] R. Suzuki *et al.*, "1-nm-capacitance-equivalent-thickness HfO_2/Al_2O_3/InGaAs metal-oxide-semiconductor structure with low interface trap density and low gate leakage current density," *Appl. Phys. Lett.*, vol. 100, no. 13, p. 132906, 2012.

[12] B. Brennan, M. Milojevic, C. L. Hinkle, F. S. Aguirre-Tostado, G. Hughes, and R. M. Wallace, "Optimisation of the ammonium sulphide $(NH_4)_2S$ passivation process on $In_{0.53}Ga_{0.47}As$," *Appl. Surf. Sci.*, vol. 257, no. 9, pp. 4082–4090, 2011.

[13] É. O'Connor *et al.*, "A systematic study of $(NH_4)_2S$ passivation (22%, 10%, 5%, or 1%) on the interface properties of the Al_2O_3/In0.53$Ga_{0.47}As$/InP system for n-type and p-type $In_{0.53}Ga_{0.47}As$ epitaxial layers," *J. Appl. Phys.*, vol. 109, no. 2, p. 024101, 2011.

[14] A. O'Mahony *et al.*, "Structural and electrical analysis of the atomic layer deposition of HfO_2/n-$In_{0.53}Ga_{0.47}As$ capacitors with and without an Al_2O_3 interface control layer," *Appl. Phys. Lett.*, vol. 97, no. 5, pp. 052904-1–052904-3, 2010.

[15] R. Engel-Herbert, Y. Hwang, and S. Stemmer, "Comparison of methods to quantify interface trap densities at dielectric/III-V semiconductor interfaces," *J. Appl. Phys.*, vol. 108, no. 12, pp. 124101-1–124101-15, 2010.

[16] B. Shin, J. R. Weber, R. D. Long, P. K. Hurley, C. G. Van de Walle, and P. C. McIntyre, "Origin and passivation of fixed charge in atomic layer deposited aluminum oxide gate insulators on chemically treated InGaAs substrates," *Appl. Phys. Lett.*, vol. 96, no. 15, pp. 152908-1–152908-3, 2010.

[17] H.-D. Trinh *et al.*, "The influences of surface treatment and gas annealing conditions on the inversion behaviors of the atomic-layer-deposition Al_2O_3/n-$In_{0.53}Ga_{0.47}As$ metal-oxide-semiconductor capacitor," *Appl. Phys. Lett.*, vol. 97, no. 4, pp. 042903-1–042903-3, 2010.

[18] É. O'Connor, S. Monaghan, K. Cherkaoui, I. M. Povey, and P. K. Hurley, "Analysis of the minority carrier response of *n*-type and *p*-type Au/Ni/Al_2O_3/$In_{0.53}Ga_{0.47}As$/InP capacitors following an optimized $(NH_4)_2S$ treatment," *Appl. Phys. Lett.*, vol. 99, no. 21, p. 212901, 2011.

[19] T. D. Lin *et al.*, "Realization of high-quality HfO_2 on $In_{0.53}Ga_{0.47}As$ by *in-situ* atomic-layer-deposition," *Appl. Phys. Lett.*, vol. 100, no. 17, p. 172110, 2012.

[20] S. Monaghan *et al.*, "Electrical analysis of three-stage passivated $In_{0.53}Ga_{0.47}As$ capacitors with varying HfO_2 thicknesses and incorporating an Al_2O_3 interface control layer," *J. Vac. Sci. Technol. B*, vol. 29, no. 1, pp. 01A807-1–01A807-8, 2011.

[21] G. Brammertz, A. Alian, D. H.-C. Lin, M. Meuris, M. Caymax, and W.-E. Wang, "A combined interface and border trap model for high-mobility substrate metal–oxide–semiconductor devices applied to $In_{0.53}Ga_{0.47}As$ and InP capacitors," *IEEE Trans. Electron Devices*, vol. 58, no. 11, pp. 3890–3897, Nov. 2011.

[22] G. Hellings *et al.*, "A fast and accurate method to study the impact of interface traps on germanium MOS performance," *IEEE Trans. Electron Devices*, vol. 58, no. 4, pp. 938–944, Apr. 2011.

[23] S. Monaghan *et al.*, "Effects of alternating current voltage amplitude and oxide capacitance on mid-gap interface state defect density extractions in $In_{0.53}Ga_{0.47}As$ capacitors," *J. Vac. Sci. Technol. B*, vol. 31, no. 1, pp. 01A119–01A127, 2013.

[24] T. P. O'Regan, P. K. Hurley, B. Sorée, and M. V. Fischetti, "Modeling the capacitance-voltage response of $In_{0.53}Ga_{0.47}As$ metal–oxide–semiconductor structures: Charge quantization and nonparabolic corrections," *Appl. Phys. Lett.*, vol. 96, no. 21, p. 213514, 2010.

[25] É. O'Connor *et al.*, "Temperature and frequency dependent electrical characterization of HfO_2/$In_xGa_{1-x}As$ interfaces using capacitance-voltage and conductance methods," *Appl. Phys. Lett.*, vol. 94, no. 10, p. 102902, 2009.

[26] G. Brammertz, H.-C. Lin, M. Caymax, M. Meuris, M. Heyns, and M. Passlack, "On the interface state density at $In_{0.53}Ga_{0.47}As$/oxide interfaces," *Appl. Phys. Lett.*, vol. 95, no. 20, p. 202109, 2009.

[27] N. Taoka *et al.*, "Impact of Fermi level pinning inside conduction band on electron mobility of $In_xGa_{1-x}As$ MOSFETs and mobility enhancement by pinning modulation," in *Proc. IEDM*, Dec. 2011, p. 610.

[28] J. J. Gu, A. T. Neal, and P. D. Ye, "Effects of $(NH_4)_2S$ passivation on the off-state performance of 3-dimensional InGaAs metal–oxide–semiconductor field-effect transistors," *J. Appl. Phys.*, vol. 99, no. 15, p. 152113, 2011.

[29] *Ioffe Physico-Technical Institute New Semiconductor Materials Characteristics and Properties*. [Online]. Available: http://www.ioffe.ru/SVA/NSM/Semicond/GaInAs/bandstr.html, accessed Jul. 16, 2014.

[30] W. Shockley and W. T. Read, Jr., "Statistics of the recombinations of holes and electrons," *Phys. Rev.*, vol. 87, no. 5, p. 835, Sep. 1952.

[31] R. N. Hall, "Electron-hole recombination in germanium," *Phys. Rev.*, vol. 87, p. 387, Jul. 1952.

[32] D. K. Schroder, "Carrier lifetimes in silicon," *IEEE Trans. Electron Devices*, vol. 44, no. 1, pp. 160–170, Jan. 1997.

[33] V. Djara *et al.*, "Impact of forming gas annealing on the performance of surface-channel $In_{0.53}Ga_{0.47}As$ MOSFETs with an ALD Al_2O_3 gate dielectric," *IEEE Trans. Electron Devices*, vol. 59, no. 4, pp. 1084–1090, Apr. 2012.

[34] J. Lin *et al.*, "An investigation of capacitance-voltage hysteresis in metal/high-*k*/$In_{0.53}Ga_{0.47}As$ metal-oxide-semiconductor capacitors," *J. Appl. Phys.*, vol. 114, no. 14, p. 144105, 2013.

[35] C. Chelli *et al.*, "Minority carrier lifetime in MOCVD-grown C- and Zn-doped InGaAs," in *Proc. 11th Int. Conf. Indium Phosph. Rel. Mater. (IPRM)*, Davos, Switzerland, May 1999, pp. 127–130.

[36] R. K. Ahrenkiel, R. Ellingson, S. Johnston, and M. Wanlass, "Recombination lifetime of $In_{0.53}Ga_{0.47}As$ as a function of doping density," *Appl. Phys. Lett.*, vol. 72, no. 26, p. 3470, 1998.

[37] R. D. L. Kronig, "On the theory of dispersion of X-rays," *J. Opt. Soc. Amer.*, vol. 12, no. 6, pp. 547–556, 1926.

[38] H. A. Kramers, "Some remarks on the theory of absorption and refraction of X-rays," *Nature*, vol. 117, no. 2952, pp. 774–775, 1926.

[39] K. J. Yang and C. Hu, "MOS capacitance measurements for high-leakage thin dielectrics," *IEEE Trans. Electron Devices*, vol. 46, no. 7, pp. 1500–1501, Jul. 1999.

[40] M. Passlack, "Off-state current limits of narrow bandgap MOSFETs," *IEEE Trans. Electron Devices*, vol. 53, no. 11, pp. 2773–2778, Nov. 2006.

[41] M. Passlack *et al.*, "Lifting the off-state bandgap limit in InAs channel metal-oxide-semiconductor heterostructures of nanometer dimensions," *Appl. Phys. Lett.*, vol. 104, no. 22, p. 223501, 2014.

Scott Monaghan (M'10–SM'13) received the B.Sc. (1^{st} Hons.) degree in mathematics and physics from Open University, Milton Keynes, in 1999, while working full-time in industry, and the M.S. and Ph.D. degrees, from University College Cork, Cork, Ireland, in 2002 and 2007, respectively, the former while working full-time in industry.

Éamon O'Connor received the B.E. degree in 2002, and the M.Eng.Sc. degree in 2005, from University College Cork, Cork, Ireland. He is currently pursuing the Ph.D. degree with Tyndall National Institute, Cork.

His research is focused on the formation of devices employing high-k dielectric materials on high-mobility III-V compound semiconductors for future CMOS applications, in particular, the passivation and characterization of electrically active defects at the high-k/III-V interface.

Eimear Ryan is currently pursuing the B.Sc. degree in mathematical sciences with the University College Cork, Cork, Ireland, who was successful in completing an Internship Award working with the team of Paul K. Hurley, Tyndall National Institute, Cork. Her internship work included mathematical applications of equivalent circuit models and solid-state electrostatic physics simulations for direct comparison to novel experimental MOS systems.

Ian M. Povey received the B.Sc. (Hons.) degree in chemistry and Ph.D. degree in spectroscopic studies of III/V semiconductor growth mechanisms from Manchester University, Manchester, U.K., in 1989 and 1994, respectively.

He became a Senior Staff Scientist with Tyndall National Institute, University College Cork, Cork, Ireland, in 2004, where he manages the atomic layer deposition activities of the Institute; studying aspects of process control, materials properties and mechanisms of growth.

Fahmida Ferdousi received the Ph.D. degree in electrical engineering from the University of Texas at Austin, Austin, TX, USA.

She is currently with Components Research, Intel Corporation, Santa Clara, CA, USA, focusing on scaled logic transistors for future technology nodes.

Rafael Rios (M'86–SM'12) received the Ph.D. degree in electrical engineering from Drexel University, Philadelphia, PA, USA.

He is currently with Intel Corporation, Santa Clara, CA, USA, working in the modeling, fabrication, and characterization of advanced semiconductor devices. He has multiple technical publications and issued patents.

Kelin J. Kuhn (M'78–SM'04–F'11) received the B.S. degree in electrical engineering from the University of Washington, Seattle, WA, USA, in 1980, and the M.S. and Ph.D. degrees in electrical engineering from Stanford University, Palo Alto, CA, USA, in 1985.

She is currently an Intel Fellow and has been involved in Intel's manufacturing process technology development for the 0.35 um, 130 nm, 90 nm, 45 nm, 22 nm, 14 nm, and 10 nm technology nodes.

Liam Floyd received the degrees in mathematical physics and pure mathematics from University College Cork (UCC), Cork, Ireland.

He is a Lecturer at UCC. He has worked with the National Microelectronics Research Centre, now Tyndall National Institute, Cork, Ireland, since 1990. He has authored or co-authored 25 papers.

Karim Cherkaoui received the Ph.D. degree from the Institut National des Sciences Appliquées of Lyon, Lyon, France, in 1998.

He joined Tyndall National Institute, University College Cork, Cork, Ireland, In 1999, where he established and developed several low-temperature electrical metrology techniques. His current research interests include the process development and characterization of high dielectric constant materials on Si and III-V materials for future metal-oxide-semiconductor devices.

Paul K. Hurley (M'93) received the Ph.D. degree in 1990 and the B.Eng. (Hons.) degree in 1985 in electronic engineering with the University of Liverpool, Liverpool, U.K.

He is a Senior Research Scientist, a Part-Time Lecturer, and the Head of the Nanoelectronic Materials and Devices Group with the Tyndall National Institute, University College Cork, Cork, Ireland.